Supplementary Notes for Quantum State Smoothing for Tracking Optical Quantum Dynamics and Recovering Purity and Squeezing

1 Experimental details

The schematic of our optical system and control paths is shown in Fig. S1. The following sections describe the optics and control systems of the experiment in detail.

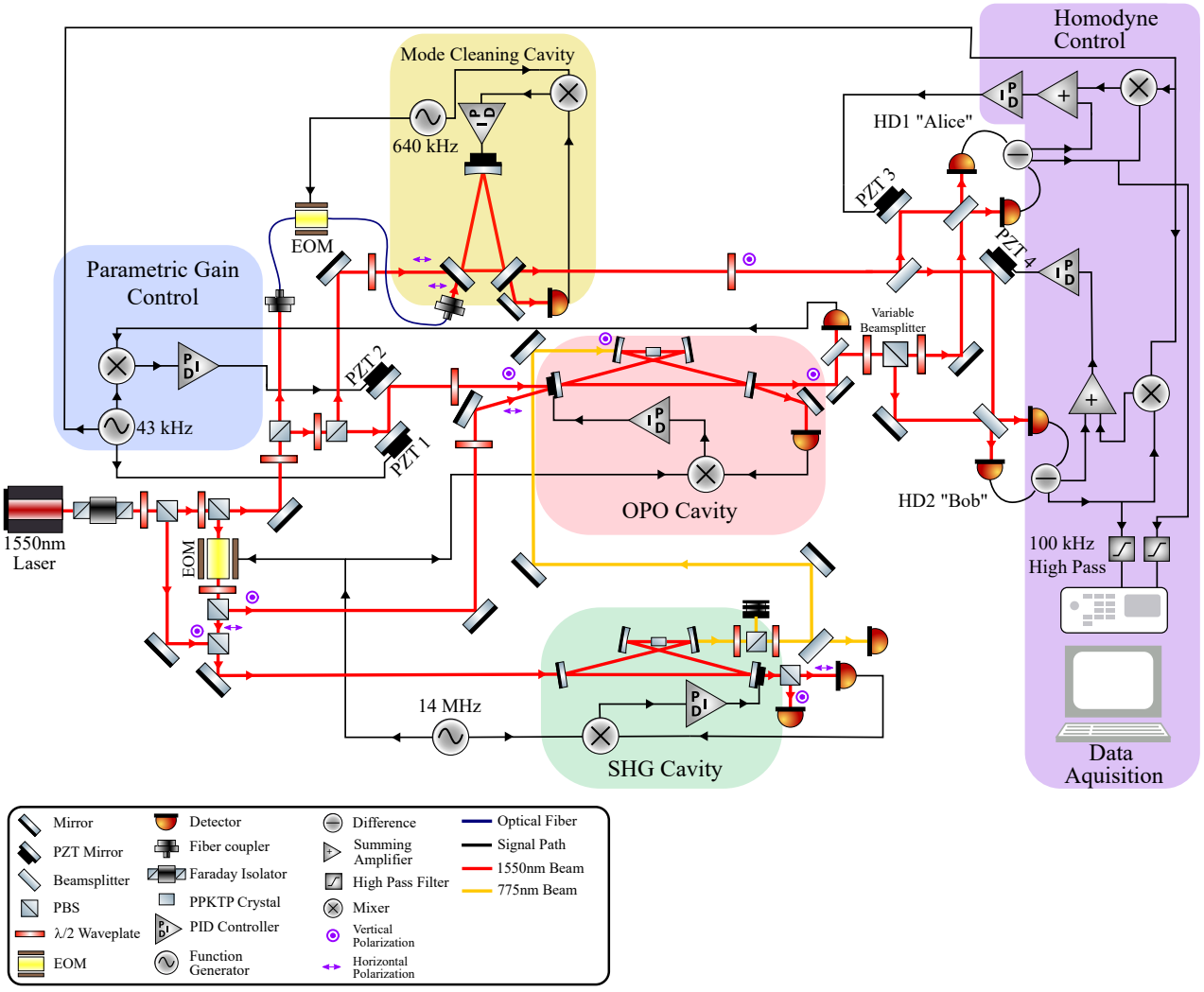


Fig. S1 A schematic of the full experimental setup, including the optical system and the control paths used to operate the experiment and take measurements. The legend in the bottom left shows what each symbol represents in the setup.

1.1 Optical system

A continuous-wave 1550 nm laser is used as the optical source for this experiment. The laser power is around 2.7 W at the source, which is split into the numerous paths as illustrated in Fig. S1.

Figure S1 shows the different optical sub-systems used in the experiment. An optical parametric oscillator (OPO) is used to prepare the quantum state (shown in red). A mode cleaning cavity (MCC) is employed to prepare a local oscillator (LO) beam that is used for homodyne detection (shown in yellow). The OPO is pumped by a 775 nm beam that is produced via second harmonic generation (SHG) from a cavity (shown in green). The squeezed beam from the OPO is split using a variable beam splitter, which is a combination of a polarizing beam splitter (PBS) and half waveplates used to control the splitting ratio. Both the transmitted and reflected beams are interfered with LO beams and then measured with homodyne detectors.

Each cavity requires a locking beam and a probe beam. Each locking beam is modulated using an electro-optic modulator (EOM) to generate sidebands that are used to lock the cavities using the Pound-Drever-Hall (PDH) technique[1]. Each cavity features a mirror mounted to a PZT, which is used to actively tune the cavity length to match the laser wavelength using feedback from the PDH error signal.

The MCC is configured as a three mirror ring cavity with the round-trip length of 800 mm which allows for spatial separation of the fields propagating clockwise and anti-clockwise at the output. The cavity is crafted out of a solid block of aluminum to provide stability, and is sealed to minimize loss. For this experiment the LO power is set to 1 mW.

The SHG cavity is a bow-tie cavity with a periodically poled potassium-titanyl-phosphate (PPKTP) crystal mounted inside. The interaction between the intracavity field and the PPKTP crystal results in second harmonic generation, which produces a beam at the double frequency of the input beam (775 nm). The crystal is mounted on a 3-axis translation stage which allows for fine control of its position. The crystal has the size of $11(\mathrm{L})\times2.5(\mathrm{W})\times1(\mathrm{H})\mathrm{mm}^3$ and two wedged surfaces (the surfaces that the beam is transmitted through) to make the shape of a trapezium. This shape allows for the effective length of the crystal that interacts with the beam to be fine tuned by moving the translation stage perpendicular to the beam. The wedged surfaces also minimize the interference of fields that are reflected off the crystal surface.

The conversion efficiency of the PPKTP crystal is temperature dependent; hence, for a given input power, the amount of light generated at 775 nm will change according to the crystal temperature. A temperature controller is used to heat the crystal inside the cavity so that we can tune this conversion efficiency. As can be seen in Fig. S1, the locking beam and probe beam for the SHG cavity use horizontal and vertical polarization, respectively (the beam polarization is indicated by a symbol in Fig. S1 as shown in the legend at the bottom of the figure). These two beams are combined on a PBS for injection into the cavity through the same port. The beams are separated by a PBS at the output port of the SHG cavity, where two different detectors are used for cavity locking and for monitoring the probe power. Since the crystal is birefringent, the crystal position and temperature can both be used to tune the resonance frequencies of the two different polarized beams to match. The phase matching temperature of the crystal has a very broad maximum which allows us to fine tune the resonance with the temperature controller without sacrificing conversion efficiency. The output power of the SHG is controlled using a variable BS (the power of 600 mW is used for the results shown in this paper), and is monitored by a detector which measures a pick-off beam in the pump path.

The OPO is another bow-tie cavity with a PPKTP crystal, which is used to generate squeezed states via spontaneous parametric down-conversion. The mechanical structure of the OPO is the same as the SHG cavity. The designed optical round-trip length of the cavity is 489 mm. The measured transmission ratio of the output coupler is 10.0%, and the intracavity loss of the OPO is 0.282%. The pump beam used for this non-linear optical process is the 775 nm beam created from the SHG cavity as described above. As with the SHG cavity, the crystal inside the OPO is positioned on a translation stage and has wedged surfaces. The conversion efficiency of the crystal is temperature dependent, and a temperature controller is used to heat the crystal in the same manner as the SHG cavity. For the OPO, the locking beam with 1 mW and probe beam use horizontal and vertical polarization, respectively, as indicated in Fig. S1. These beams are injected through the same mirror, but are injected at different angles so that they propagate in opposite directions around the cavity. This allows spatial separation of the locking and probe beams as they leave the cavity, meaning that the locking beam does not contaminate the OPO probe output, and can be detected separately. The probe power is 80 nW at the output so that the interference signal with an LO beam does not saturate at the homodyne detector. As with the SHG cavity, the temperature and crystal position can both be tuned to match the resonance frequencies of the locking and probe beams. For the measurements presented in this paper, the pump beam power is set to 600 mW, resulting in a parametric gain of $G_+ = 11.4$.

A 99% reflective beam splitter is used to pick off 1% of the OPO probe beam output. This measured probe output is fed back to the relative phase of the probe beam through PZT 2 (see Fig. S1) in the OPO input path. A PBS is used along with a half waveplate to split the OPO output to the two homodyne detectors. The homodyne detectors are custom made with a quantum efficiency specification of 99%. The detector consists of a transimpedance amplifier with 39 kΩ, a cascade buffer amplifier, and a high-pass filter with the cutoff frequency of 8 kHz in between them. The clearance, the ratio between shot noise and detector electronic noise, is about −25 dB on average in the range from 1 MHz to 5 MHz with 1 mW LO power. The LO and OPO outputs are mode-matched to each other, with a typical visibility of 99.3%. The propagation loss in these detection paths from the OPO output has been measured at 8.4% for Alice and 8.8% for Bob.

The experimental parameters used for quantum state smoothing are listed in Table S1 and Table S2. Here $c = 3 \times 10^8$ m/s is the speed of light in the vacuum. Note that η_{m0} corresponds to the total measurement efficiency without the transmission ratio of the variable beamsplitter T,

$$\eta_{A0} = \frac{\eta_{\mathrm{A}}}{T}, \qquad \eta_{B0} = \frac{\eta_{\mathrm{B}}}{1-T}, \tag{S1}$$

where η_{A} and η_{B} are defined by Eq. (S13).

1.2 System control

As mentioned in Section 1.1, the three cavities are locked using the PDH technique with modulated locking beams. These control loops can be seen in Fig. S1, with the control loops for the SHG cavity, OPO, and MCC highlighted in green, red, and yellow, respectively.

A modulation frequency of 14 MHz is used for the free space EOM in the bottom left of Fig. S1 to produce sidebands for locking the SHG and OPO cavities. For the fiber EOM, a modulation frequency of 640 kHz is used for modulating the locking beam of the mode cleaning cavity.

The parametric gain is controlled by modulating a PZT mirror with the frequency of 43 kHz in the input path of the OPO probe beam (PZT 1 in Fig. S1). This modulation signal is then mixed with a detected signal at the output of the OPO cavity to create an error signal that is injected into a servo which actuates on PZT 2 in the OPO probe input path. This actuation controls the relative phase of the probe and pump beams in the OPO which controls the parametric gain. This configuration is illustrated in Fig. S1, with control paths for the parametric gain control highlighted in blue.

For each of the homodyne detectors, a PZT mirror is used in the LO path to control the relative phase between the squeezed beam and the LO beam when they interfere (PZT 3 is used for 'Alice' and PZT 4 is used for 'Bob'). By controlling this phase it is possible to tune the measurement angle of the detector. The error signal for this control loop is created by summing together two components: the DC signal from the homodyne detector, and the demodulated AC signal. These components individually can be used as an error signal to lock to either a squeezing (90° measurement angle) or anti-squeezing (0° angle) measurement. By combining them it is possible to lock the homodyne detector to any angle by simply tuning the relative gains of these

Table S1 Parameters regarding OPO.

Cavity parameters	Variable	Value
Parametric gain	G_+	11.4
Normalized pump amplitude	$\xi = 1 - 1/\sqrt{G_+}$	0.70
Optical round-trip length	l	489 mm
Output coupler	T_c	10.0%
Intracavity loss	L_c	0.282%
Half width at half maximum	$f_{\mathrm{HWHM}} = \gamma/(2\pi) = c(T_c + L_c)/(4\pi l)$	5.0 MHz
Escape efficiency	$\eta_c = T_c/(T_c + L_c)$	97.3%

Table S2 Parameters regarding efficiency.

Efficiency parameters	Variable	Alice	Bob
Visibility	ζ_m	99.2%	99.3%
Propagation loss	$1 - \eta_m^{(\mathrm{prop})}$	8.4%	8.8%
Shot noise clearance (1 MHz – 5 MHz)	$1 - \eta_m^{(\mathrm{elec})}$	−25.4 dB	−25.6 dB
Quantum efficiency of photodiode	$\eta_m^{(\mathrm{PD})}$	99%	99%
Total efficiency without T	$\eta_{m0} = \eta_c \zeta_m^2 \eta_m^{(\mathrm{prop})} \eta_m^{(\mathrm{elec})} \eta_m^{(\mathrm{PD})}$	86.5%	86.3%

two signals. Figure S1 shows this control configuration highlighted in purple. The measurement control loop has a phase noise of around $\pm 2°$.

The signals from the homodyne detectors are measured using a Tektronix DPO7104 Digital Phosphor Oscilloscope. These signals are passed through the fifth-order Butterworth high-pass filter with the cutoff frequency of 100 kHz before measurement to remove a signal that is observed from the 43 kHz PZT frequency. These measurements are recorded at 1 GS/s for a duration of 10 ms or 50 µs to be used as data for estimation of the state dynamics.

2 Theoretical calculations

2.1 Detailed experimental model

In Fig. S2, we show our experimental model of the OPO system involving all the necessary parameters required. The annihilation (creation) operator describing the intra-cavity mode is denoted by $\hat{a}$ ($\hat{a}^\dagger$). The intra-cavity loss is modelled by a partially-reflective mirror (lower left in the cavity) with transmissivity L_c. There is an additional partially-reflective mirror, with transmissivity T_c, whose output is used for measurement. The decay rate of the cavity mode due to the intra-cavity loss and the output coupler, respectively, are given by

$$\gamma_{L_c} = \frac{c}{l} L_c \qquad \text{and} \qquad \gamma_{T_c} = \frac{c}{l} T_c \,, \tag{S2}$$

where c is the speed of light and l is the round-trip length of the cavity.

The Hamiltonian of the degenerate OPO is given as[2],

$$\hat{\mathcal{H}} = \hbar\omega_c \hat{a}^\dagger \hat{a} + \frac{i\hbar}{2}\left[\epsilon \mathrm{e}^{-i\omega_p t}(\hat{a}^\dagger)^2 - \epsilon^* \mathrm{e}^{i\omega_p t}\hat{a}^2\right], \tag{S3}$$

where ω_c is the resonance frequency of the cavity, $\omega_p = 2\omega_c$ is the frequency of the beam pumping the cavity which has an amplitude of $\epsilon \in \mathbb{R}$. Moving to a rotating frame with respect to $\hbar\omega_c \hat{a}^\dagger \hat{a}$, the Hamiltonian becomes

$$\hat{\mathcal{H}}^{\mathrm{RF}} = \frac{i\hbar}{2}\epsilon[(\hat{a}^\dagger)^2 - \hat{a}^2]\,. \tag{S4}$$

Using standard input-output theory[2, 3], we obtain the Heisenberg equation of motion for the cavity mode,

$$\begin{aligned} \frac{d\hat{a}}{dt} &= -\frac{i}{\hbar}[\hat{a}(t), \hat{\mathcal{H}}^{\mathrm{RF}}] - \gamma\hat{a}(t) + \sqrt{\gamma_{L_c}}\hat{b}_1^{(0)}(t) + \sqrt{\gamma_{T_c}}\hat{b}_2^{(0)}(t) \\ &= \epsilon\hat{a}^\dagger(t) - \gamma\hat{a}(t) + \sqrt{\gamma_{L_c}}\hat{b}_1^{(0)}(t) + \sqrt{\gamma_{T_c}}\hat{b}_2^{(0)}(t)\,, \end{aligned} \tag{S5}$$

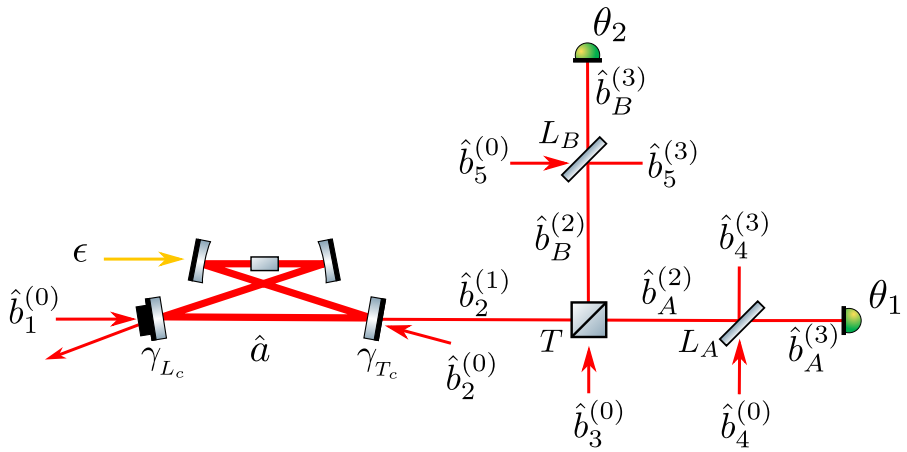


Fig. S2 The schematics of our detailed experimental model. An OPO with injected pump amplitude ϵ. Vacuum inputs to the system are shown as $\hat{b}_j^{(0)} (j = 1, \ldots, 5)$. Homodyne measurements are shown by the measurement phases θ_1 and θ_2. γ_{L_c} and γ_{T_c} are the decay rate given by intracavity loss L_c and output coupler transmission T_c. L_A and L_B represent measurement losses. T is the transmission ratio of a variable beam splitter.

where

$$\gamma = \frac{1}{2}(\gamma_{L_c} + \gamma_{T_c})\,. \tag{S6}$$

The operators $\hat{b}_j^{(0)}$ are annihilation operators describing the input field at each partially-reflective mirror. The field at each mirror is assumed independent, with $[\hat{b}_j^{(0)}(t), \hat{b}_{j'}^{(0)}(t')] = 0$ and $[\hat{b}_j^{(0)}(t), (\hat{b}_{j'}^{(0)}(t'))^\dagger] = \delta(t-t')\delta_{j,j'}$ (see Fig. S2 for our numbering conventions for j), and the superscript zero denotes a vacuum field. It is also convenient to introduce the infinitesimal noise operator $d\hat{B}_j^{(0)}(t) = \hat{b}_j^{(0)}(t)dt$, where $[d\hat{B}_j^{(0)}(t), (d\hat{B}_j^{(0)}(t'))^\dagger] = \delta(t-t')\mathrm{d}t^2$. With this noise operator introduced, dynamics of the cavity is described by the stochastic differential equation

$$d\hat{a} = \epsilon\hat{a}^\dagger dt - \gamma\hat{a}dt + \sqrt{\gamma_{L_c}}d\hat{B}_1^{(0)} + \sqrt{\gamma_{T_c}}d\hat{B}_2^{(0)}\,, \tag{S7}$$

where, for simplicity, we have dropped the time argument, and from this point on-wards unless necessary. With this, we have the dynamics of the system. Before we write these dynamics in a standard form involving the canonical position and momentum operators, we will address Alice's and Bob's measurements.

To determine the operators that Alice and Bob are (effectively) measuring, we need to know how the output field $\hat{b}_2^{(1)}$ is related to the intra-cavity field. From the input-output calculation earlier, we have

$$\hat{b}_2^{(1)} = \sqrt{\gamma_{T_c}}\hat{a} - \hat{b}_2^{(0)}\,. \tag{S8}$$

From Fig. S2, this output field encounters a variable beam splitter, with transmissivity T, which divides the output into a portion that is observed by Alice and another by Bob. The output fields from this beam splitter are given by the transformation

$$\begin{pmatrix}\hat{b}_{\mathrm{A}}^{(2)}\\ \hat{b}_{\mathrm{B}}^{(2)}\end{pmatrix} = \begin{pmatrix}\sqrt{T} & -\sqrt{1-T}\\ \sqrt{1-T} & \sqrt{T}\end{pmatrix}\begin{pmatrix}\hat{b}_2^{(1)}\\ \hat{b}_3^{(0)}\end{pmatrix}\,, \tag{S9}$$

where the second input to the beam splitter is an independent vacuum field with annihilation operator $\hat{b}_3^{(0)}$. The output fields are then sent to Alice and Bob who each perform a homodyne measurement. However, there is additional loss that is experienced along each path. This is modelled in the standard way by introducing a beam splitter in each arm whose reflectivity corresponds to the fraction of the field lost, L_m. Thus, the fields that Alice and Bob, respectively, obtain are

$$\begin{pmatrix}\hat{b}_{\mathrm{A}}^{(3)}\\ \hat{b}_4^{(3)}\end{pmatrix} = \begin{pmatrix}\sqrt{1-L_{\mathrm{A}}} & -\sqrt{L_{\mathrm{A}}}\\ \sqrt{L_{\mathrm{A}}} & \sqrt{1-L_{\mathrm{A}}}\end{pmatrix}\begin{pmatrix}\hat{b}_{\mathrm{A}}^{(2)}\\ \hat{b}_4^{(0)}\end{pmatrix}\,, \tag{S10}$$

$$\begin{pmatrix}\hat{b}_{\mathrm{B}}^{(3)}\\ \hat{b}_5^{(3)}\end{pmatrix} = \begin{pmatrix}\sqrt{1-L_{\mathrm{B}}} & -\sqrt{L_{\mathrm{B}}}\\ \sqrt{L_{\mathrm{B}}} & \sqrt{1-L_{\mathrm{B}}}\end{pmatrix}\begin{pmatrix}\hat{b}_{\mathrm{B}}^{(2)}\\ \hat{b}_5^{(0)}\end{pmatrix}\,. \tag{S11}$$

Note, $1-L_m$ corresponds to the measurement efficiency *without* the escape efficiency from a cavity, and is determined via

$$1 - L_m = \zeta_m^2\eta_m^{(\mathrm{prop})}\eta_m^{(\mathrm{elec})}\eta_m^{(\mathrm{PD})}, \tag{S12}$$

with the efficiency parameters: ζ, visibility between a probe and an LO; $\eta^{(\mathrm{prop})}$, optical propagation efficiency; $1-\eta^{(\mathrm{elec})}$, the ratio of electrical noise power to shot noise power; and $\eta^{(\mathrm{PD})}$, quantum efficiency of the photodiodes.

The overall measurement efficiency for both Alice and Bob, including the escape efficiency of the cavity, is given by

$$\eta_A = \eta_c(1-L_{\mathrm{A}})T \qquad \text{and} \qquad \eta_{\mathrm{B}} = \eta_c(1-L_{\mathrm{B}})(1-T)\,, \tag{S13}$$

with $\eta_c = \gamma_{T_c}/(\gamma_{T_c}+\gamma_{L_c})$. After computing all the beam splitters along Alice's and Bob's paths, the fields that they receive in terms of the intra-cavity mode are

$$\hat{b}_{\mathrm{A}}^{(3)} = \sqrt{2\gamma\eta_{\mathrm{A}}}\hat{a} - \sqrt{(1-L_{\mathrm{A}})T}\hat{b}_2^{(0)} - \sqrt{(1-L_{\mathrm{A}})(1-T)}\hat{b}_3^{(0)} - \sqrt{L_{\mathrm{A}}}\hat{b}_4^{(0)}\,, \tag{S14}$$

$$\hat{b}_{\mathrm{B}}^{(3)} = \sqrt{2\gamma\eta_{\mathrm{B}}}\hat{a} - \sqrt{(1-L_{\mathrm{B}})(1-T)}\hat{b}_2^{(0)} + \sqrt{(1-L_{\mathrm{B}})T}\hat{b}_3^{(0)} - \sqrt{L_{\mathrm{B}}}\hat{b}_5^{(0)}\,. \tag{S15}$$

With the field present at both Alice's and Bob's detectors, we can compute the operator corresponding to their homodyne measurement. The procedure of homodyne measurement is briefly explained as follows. The input field is mixed with a strong classical field, called a local oscillator (LO), on a balanced beam-splitter, whereby each output is measured using a photodetector. The difference in the measured intensities of the two photodetectors gives the result of the homodyne measurement, up to a constant. We take the state of the strong LO to be a coherent state $|\beta e^{i\theta_m}\rangle$ with $\beta \in \mathbb{R}$ large enough so that the quantum fluctuations in both β and θ_m are negligible. Here β^2 is the photon flux of the beam and θ_m its phase; $m = A, B$ depending on whether we are considering Alice's or Bob's measurement. Under this assumption, we can replace the annihilation operator describing the LO with its expectation value $\beta e^{i\theta_m}$. Thus, after the balanced beam-splitter, we have

$$\begin{pmatrix} \hat{c}_m \\ \hat{d}_m \end{pmatrix} = \frac{1}{\sqrt{2}} \begin{pmatrix} 1 & -1 \\ 1 & 1 \end{pmatrix} \begin{pmatrix} \hat{b}_m^{(3)} \\ \beta e^{i\theta_m} \end{pmatrix}. \tag{S16}$$

The intensities of the beams at the detectors are $\hat{c}_m^\dagger \hat{c}_m$ and $\hat{d}_m^\dagger \hat{d}_m$. Thus, the operator describing Alice's and Bob's homodyne measurement is

$$\hat{y}_m = \beta^{-1}(\hat{d}_m^\dagger \hat{d}_m - \hat{c}_m^\dagger \hat{c}_m) = e^{-i\theta_m}\hat{b}_m^{(3)} + e^{i\theta_m}(\hat{b}_m^{(3)})^\dagger \,. \tag{S17}$$

We now introduce the canonical position and momentum operators for the cavity field, defined as

$$\hat{x} = \sqrt{\frac{\hbar}{2}}(\hat{a} + \hat{a}^\dagger)\,, \qquad \hat{p} = i\sqrt{\frac{\hbar}{2}}(\hat{a}^\dagger - \hat{a})\,, \tag{S18}$$

and for the normalized noise quadrature operators

$$d\hat{x}_j^{(0)} = \left(d\hat{B}_j^{(0)} + (d\hat{B}_j^{(0)})^\dagger\right), \qquad d\hat{p}_j^{(0)} = i\left((d\hat{B}_j^{(0)})^\dagger - d\hat{B}_j^{(0)}\right). \tag{S19}$$

Note, these noise quadrature operators are normalized such that

$$\langle d\hat{x}_j^{(0)}\rangle = 0\,, \qquad \text{and} \qquad \langle (d\hat{x}_j^{(0)})^2\rangle = dt\,, \tag{S20}$$

where the expectation is taken with the vacuum state in the j-th mode, and similarly for $d\hat{p}_j^{(0)}$. With these operators, the equations for the system become

$$d\hat{\mathbf{x}} = A\hat{\mathbf{x}}dt + Bd\hat{\mathbf{v}}\,, \tag{S21}$$

$$\hat{y}_m dt = C_m\hat{\mathbf{x}}dt + D_m d\hat{\mathbf{v}}\,, \tag{S22}$$

where

$$\hat{\mathbf{x}} \equiv \begin{pmatrix}\hat{x} & \hat{p}\end{pmatrix}^\top, \tag{S23}$$

$$d\hat{\mathbf{v}} \equiv \left(d\hat{x}_1^{(0)} \;\; d\hat{p}_1^{(0)} \;\; \ldots \;\; d\hat{x}_5^{(0)} \;\; d\hat{p}_5^{(0)}\right)^\top. \tag{S24}$$

The matrices are

$$A = \begin{pmatrix} -\gamma(1-\xi) & 0 \\ 0 & -\gamma(1+\xi) \end{pmatrix}, \tag{S25}$$

$$B = \sqrt{\frac{\hbar}{2}} \begin{pmatrix} \sqrt{\gamma_{L_c}} & 0 & \sqrt{\gamma_{T_c}} & 0 & 0\;0\;0\;0\;0\;0 \\ 0 & \sqrt{\gamma_{L_c}} & 0 & \sqrt{\gamma_{T_c}} & 0\;0\;0\;0\;0\;0 \end{pmatrix}, \tag{S26}$$

$$C_m = \sqrt{\frac{4\gamma\eta_m}{\hbar}}\begin{pmatrix}\cos\theta_m & \sin\theta_m\end{pmatrix}, \tag{S27}$$

$$D_m = \begin{pmatrix} 0 & 0 & D_{2,c}^{(m)} & D_{2,s}^{(m)} & D_{3,c}^{(m)} & D_{3,s}^{(m)} & D_{4,c}^{(m)} & D_{4,s}^{(m)} & D_{5,c}^{(m)} & D_{5,s}^{(m)} \end{pmatrix}, \tag{S28}$$

where we use the normalized pump amplitude $\xi = \epsilon/\gamma \in [0, 1)$, given from the parametric gain G_+ as $\xi = 1 - 1/\sqrt{G_+}$, and

$$\begin{aligned}
D^{(m)}_{j,c} &= d^{(m)}_j \cos\theta_m, & D^{(m)}_{j,s} &= d^{(m)}_j \sin\theta_m, \\
d^{(A)}_2 &= -\sqrt{(1-L_\mathrm{A})T}, & d^{(B)}_2 &= -\sqrt{(1-L_\mathrm{B})(1-T)}, \\
d^{(A)}_3 &= -\sqrt{(1-L_\mathrm{A})(1-T)}, & d^{(B)}_3 &= \sqrt{(1-L_\mathrm{B})T}, \\
d^{(A)}_4 &= -\sqrt{L_\mathrm{A}}, & d^{(B)}_4 &= 0, \\
d^{(A)}_5 &= 0, & d^{(B)}_5 &= -\sqrt{L_\mathrm{B}}.
\end{aligned} \tag{S29}$$

The covariances of the noise vectors (w.r.t. a vacuum state in each mode) are

$$Q dt = \mathrm{Cov}(B d\hat{\mathbf{v}}, B d\hat{\mathbf{v}}) = \hbar\gamma I_2 dt, \tag{S30}$$

$$R_m dt = \mathrm{Cov}(D_m d\hat{\mathbf{v}}, D_m d\hat{\mathbf{v}}) = dt, \tag{S31}$$

$$S_m dt = \mathrm{Cov}(D_m d\hat{\mathbf{v}}, B d\hat{\mathbf{v}}) = -\frac{\hbar}{2} C_m dt, \tag{S32}$$

where I_k is the $k \times k$ identity matrix. Note that the noise of Alice's measurement is uncorrelated with the noise of Bob's measurement, i.e.,

$$\langle (D_\mathrm{A} d\hat{\mathbf{v}}) D_\mathrm{B} d\hat{\mathbf{v}} \rangle = 0\,. \tag{S33}$$

2.2 Quantum filtering and smoothing equations

Equations (S21) and (S22) are *linear* Langevin equations. This means that, provided the cavity begins in a Gaussian state, this system is a linear Gaussian quantum system[4]. As such, we can utilize the linear Gaussian quantum state smoothing theory. See Ref.[5] for the complete derivation of the equations that are to follow. The quantum state of a continuous-variable quantum system can be represented in many different ways. In our case we are interested in the Wigner function[4, 6], which for a linear Gaussian quantum system is a Gaussian distribution $W(\mathbf{x}) = g(\mathbf{x}; \langle\hat{\mathbf{x}}\rangle, V)$, where the state is completely parameterized by the mean $\langle\hat{\mathbf{x}}\rangle$ and covariance V. This means that, for any estimate of the state of the system, we only need to estimate the mean and covariance matrix.

The true mean $\langle\hat{\mathbf{x}}\rangle_\mathrm{T}$ and covariance V_T, that is, the mean and covariance conditioned both Alice's and Bob's measurement outcomes, evolve according to the following:

$$d\langle\hat{\mathbf{x}}\rangle_\mathrm{T} = A\langle\hat{\mathbf{x}}\rangle_\mathrm{T} dt + \left(V_\mathrm{T} C_\mathrm{A}^\top + S_\mathrm{A}\right) R_\mathrm{A}^{-1} dw_\mathrm{A} + \left(V_\mathrm{T} C_\mathrm{B}^\top + S_\mathrm{B}\right) R_\mathrm{B}^{-1} dw_\mathrm{B}, \tag{S34}$$

$$\begin{aligned}
\frac{dV_\mathrm{T}}{dt} = {} & A V_\mathrm{T} + V_\mathrm{T} A^\top + Q - \left(V_\mathrm{T} C_\mathrm{A}^\top + S_\mathrm{A}\right) R_\mathrm{A}^{-1} \left(V_\mathrm{T} C_\mathrm{A}^\top + S_\mathrm{A}\right)^\top \\
& - \left(V_\mathrm{T} C_\mathrm{B}^\top + S_\mathrm{B}\right) R_\mathrm{B}^{-1} \left(V_\mathrm{T} C_\mathrm{B}^\top + S_\mathrm{B}\right)^\top .
\end{aligned} \tag{S35}$$

Here, Alice's innovation term dw_A is an infinitesimal Wiener increment, defined as $dw_\mathrm{A} = y_\mathrm{A} dt - C_\mathrm{A}\langle\hat{\mathbf{x}}\rangle_\mathrm{T} dt$ with y_A being the outcome Alice obtains by measuring $\hat{y}_\mathrm{A}$. Bob's innovation is defined similarly. The Wiener increments satisfy the following relations

$$\mathbb{E}[dw_m(t)] = 0\,, \qquad dw_m(t) dw_{m'}(t') = \delta_{m,m'} \delta(t - t') dt^2\,, \tag{S36}$$

for $m = A, B$. The mean $\langle\hat{\mathbf{x}}\rangle_\mathrm{F}$ and covariance V_F for Alice's filtered estimate are given by

$$d\langle\hat{\mathbf{x}}\rangle_\mathrm{F} = A\langle\hat{\mathbf{x}}\rangle_\mathrm{F} dt + \left(V_\mathrm{F} C_\mathrm{A}^\top + S_\mathrm{A}\right) R_\mathrm{A}^{-1} dw_\mathrm{F}, \tag{S37}$$

$$\frac{dV_\mathrm{F}}{dt} = A V_\mathrm{F} + V_\mathrm{F} A^\top + Q - \left(V_\mathrm{F} C_\mathrm{A}^\top + S_\mathrm{A}\right) R_\mathrm{A}^{-1} \left(V_\mathrm{F} C_\mathrm{A}^\top + S_\mathrm{A}\right)^\top . \tag{S38}$$

$\langle\hat{\mathbf{x}}\rangle_\mathrm{F}$ and V_F are the mean and covariance of the filtered state and $dw_\mathrm{F} = y_\mathrm{A} dt - C_\mathrm{A}\langle\hat{\mathbf{x}}\rangle_\mathrm{F} dt$. The retrofiltering equations, using only Alice's future measurement information, are

$$-d\langle\hat{\mathbf{x}}\rangle_\mathrm{R} = -A\langle\hat{\mathbf{x}}\rangle_\mathrm{R} dt + \left(V_\mathrm{R} C_\mathrm{A}^\top - S_\mathrm{A}\right) R_\mathrm{A}^{-1} dw_\mathrm{R}, \tag{S39}$$

$$-\frac{dV_\mathrm{R}}{dt} = -A V_\mathrm{R} - V_\mathrm{R} A^\top + Q - \left(V_\mathrm{R} C_\mathrm{A}^\top - S_\mathrm{A}\right) R_\mathrm{A}^{-1} \left(V_\mathrm{R} C_\mathrm{A}^\top - S_\mathrm{A}\right)^\top , \tag{S40}$$

where $\langle\hat{\mathbf{x}}\rangle_{\mathrm{R}}$ and V_{R} are the mean and covariance of a positive operator-valued measure (POVM) element for the future record, called the retrofiltered effect. Here, the retrofiltered innovation is $dw_{\mathrm{R}} = y_{\mathrm{A}}dt - C_{\mathrm{A}}\langle\hat{\mathbf{x}}\rangle_{\mathrm{R}}dt$.

Finally, the smoothed estimate of the state, using both past and future records, is calculated via

$$\langle\hat{\mathbf{x}}\rangle_{\mathrm{S}} = (V_{\mathrm{S}} - V_{\mathrm{T}})\left[(V_{\mathrm{F}} - V_{\mathrm{T}})^{-1}\langle\hat{\mathbf{x}}\rangle_{\mathrm{F}} + (V_{\mathrm{R}} + V_{\mathrm{T}})^{-1}\langle\hat{\mathbf{x}}\rangle_{\mathrm{R}}\right], \tag{S41}$$

$$V_{\mathrm{S}} = \left[(V_{\mathrm{F}} - V_{\mathrm{T}})^{-1} + (V_{\mathrm{R}} + V_{\mathrm{T}})^{-1}\right]^{-1} + V_{\mathrm{T}}. \tag{S42}$$

$\langle\hat{\mathbf{x}}\rangle_{\mathrm{S}}$ and V_{S} are the mean and covariance of the smoothed state. Note that these equations are derived by considering the Bayesian estimation with regard to $\langle\hat{\mathbf{x}}\rangle_{\mathrm{T}}$, meaning $\langle\hat{\mathbf{x}}\rangle_{\mathrm{F}}$, $\langle\hat{\mathbf{x}}\rangle_{\mathrm{R}}$, and $\langle\hat{\mathbf{x}}\rangle_{\mathrm{S}}$ are the best estimate of $\langle\hat{\mathbf{x}}\rangle_{\mathrm{T}}$ using only past, only future, and both past and future records, respectively. The sum of the covariance of the true state V_{T} and the estimation error matrices $V_{\mathrm{F}} - V_{\mathrm{T}}$, $V_{\mathrm{R}} + V_{\mathrm{T}}$, and $V_{\mathrm{S}} - V_{\mathrm{T}}$, gives the covariances of the estimated state V_{F}, V_{R}, and V_{S}.

Smoothing equations for numerical calculations

In the previous smoothing equations, there are a couple of subtleties that need to be discussed in order to perform numerical calculations. To compute the smoothed state, one needs to calculate two matrix inverses, with the most problematic being $(V_{\mathrm{F}} - V_{\mathrm{T}})^{-1}$. This is because, especially at the initial time t_0, the matrix can be singular, i.e., $\det(V_{\mathrm{F}} - V_{\mathrm{T}}) = 0$. We can resolve this issue by algebraic manipulation of Eqs. (S41) and (S42), yielding,

$$\langle\hat{\mathbf{x}}\rangle_{\mathrm{S}} = \left[I + (V_{\mathrm{F}} - V_{\mathrm{T}})(V_{\mathrm{R}} + V_{\mathrm{T}})^{-1}\right]^{-1}\left[\langle\hat{\mathbf{x}}\rangle_{\mathrm{F}} + (V_{\mathrm{F}} - V_{\mathrm{T}})(V_{\mathrm{R}} + V_{\mathrm{T}})^{-1}\langle\hat{\mathbf{x}}\rangle_{\mathrm{R}}\right], \tag{S43}$$

$$V_{\mathrm{S}} = \left[I + (V_{\mathrm{F}} - V_{\mathrm{T}})(V_{\mathrm{R}} + V_{\mathrm{T}})^{-1}\right]^{-1}(V_{\mathrm{F}} - V_{\mathrm{T}}) + V_{\mathrm{T}}, \tag{S44}$$

where I is the identity matrix with the same dimension as V. Note, this issue is unlikely to occur in a real system with the $(V_{\mathrm{R}} + V_{\mathrm{T}})^{-1}$ term, since, for this term to be singular, would require the true state to have an infinite amount of squeezing.

The second subtlety is with the final condition on the retrofiltered effect, i.e., $V_{\mathrm{R}}(t_f) = \infty$. While the infinity is, in principle, numerically problematic, there is a deeper problem, namely, what is the final condition on the retrofiltered mean? From a theoretical perspective the final condition on the mean is meaningless as, with an infinite covariance, the Gaussian distribution becomes the uniform distribution over the real numbers. However, in a numerical computation, one would need to choose an exceedingly large but nevertheless finite value for the final covariance and the choice of $\langle\hat{\mathbf{x}}\rangle_{\mathrm{R}}$ will matter. This issue can be avoided by instead solving the new quantities

$$\breve{\Lambda}_{\mathrm{R}} \equiv (V_{\mathrm{R}} + V_{\mathrm{T}})^{-1}, \tag{S45}$$

$$\breve{\mathbf{z}}_{\mathrm{R}} \equiv \breve{\Lambda}_{\mathrm{R}}\langle\hat{\mathbf{x}}\rangle_{\mathrm{R}}, \tag{S46}$$

which have final conditions $\breve{\mathbf{z}}_{\mathrm{R}}(t_f) = 0$, $\breve{\Lambda}_{\mathrm{R}}(t_f) = 0$. Note, for consistency with the literature, we are using the notation of Refs.[5, 7]. By calculating the derivatives of $\breve{\mathbf{z}}_{\mathrm{R}}$ and $\breve{\Lambda}_{\mathrm{R}}$ with respect to time, and using Eqs. (S34), (S35), (S39) and (S40), we obtain:

$$-d\breve{\mathbf{z}}_{\mathrm{R}} = \left(\bar{A}^{\top} - \breve{\Lambda}_{\mathrm{R}}\bar{Q}\right)\breve{\mathbf{z}}_{\mathrm{R}}dt + \left[C_{\mathrm{A}}^{\top} - \breve{\Lambda}_{\mathrm{R}}(V_{\mathrm{T}}C_{\mathrm{A}}^{\top} + S_{\mathrm{A}})\right]R_{\mathrm{A}}^{-1}y_{\mathrm{A}}dt, \tag{S47}$$

$$-\frac{d\breve{\Lambda}_{\mathrm{R}}}{dt} = \breve{\Lambda}_{\mathrm{R}}\bar{A} + \bar{A}^{\top}\breve{\Lambda}_{\mathrm{R}} - \breve{\Lambda}_{\mathrm{R}}\bar{Q}\breve{\Lambda}_{\mathrm{R}} + C_{\mathrm{A}}^{\top}R_{\mathrm{A}}^{-1}C_{\mathrm{A}}, \tag{S48}$$

where

$$\bar{A} = A - \left(V_{\mathrm{T}}C_{\mathrm{A}}^{\top} + S_{\mathrm{A}}\right)R_{\mathrm{A}}^{-1}C_{\mathrm{A}}, \tag{S49}$$

$$\bar{Q} = \left(V_{\mathrm{T}}C_{\mathrm{B}}^{\top} + S_{\mathrm{B}}\right)R_{\mathrm{B}}^{-1}\left(V_{\mathrm{T}}C_{\mathrm{B}}^{\top} + S_{\mathrm{B}}\right)^{\top}. \tag{S50}$$

After this transformation, Eqs. (S43) and (S44) become

$$\langle\hat{\mathbf{x}}\rangle_{\mathrm{S}} = \left[I + (V_{\mathrm{F}} - V_{\mathrm{T}})\breve{\Lambda}_{\mathrm{R}}\right]^{-1}\left[\langle\hat{\mathbf{x}}\rangle_{\mathrm{F}} + (V_{\mathrm{F}} - V_{\mathrm{T}})\breve{\mathbf{z}}_{\mathrm{R}}\right], \tag{S51}$$

$$V_{\rm S} = \left[I + (V_{\rm F} - V_{\rm T})\bar{\Lambda}_{\rm R}\right]^{-1}(V_{\rm F} - V_{\rm T}) + V_{\rm T} \tag{S52}$$

$$= V_{\rm T} + (V_{\rm F} - V_{\rm T})\left[I + \bar{\Lambda}_{\rm R}(V_{\rm F} - V_{\rm T})\right]^{-1}. \tag{S53}$$

2.3 Theory for Figs. 4-6

To compute the theory lines in each of the figures, one needs access to three covariance matrices, $V_{\rm F}$, $V_{\rm T}$ and $\bar{\Lambda}_{\rm R}$. For the filtered covariance, one needs to solve Eq. (S38) under the steady state condition, i.e., $\mathrm{d}V_{\rm F}/\mathrm{d}t = 0$. For each plot we solve this equation for each value of θ_A and η_A specified. Similarly, for $V_{\rm T}$ and $\bar{\Lambda}_{\rm R}$, one needs to solve Eq. (S35) and (S48), respectively, using the specified values of θ_A, θ_B, $\eta_A = 0.865T$ and $\eta_B = 0.863(1-T)$ for $T \in [0,1]$. From this, one can compute $V_{\rm S}$ using Eq. (S53). Note, in solving the true state using the $\eta_A + \eta_B < 1$, the resulting true state will be impure. Furthermore, the filtered state and true state will coincide when $\eta_B = 0$, as this is when the true state is computed using only Alice's measurement record. This is seen in Fig. 4, where the filtered, smoothed and true state theory lines coincide at $\eta_A = 0.865$.

To compute the theoretical purity, one uses $\mathcal{P}(\rho_c) = 1/\sqrt{\det(2V_c/\hbar)}$ for $c = \mathrm{F},\ \mathrm{S},\ \mathrm{T}$. For the squeezing (antisqueezing), one finds the smallest (largest) eigenvalue of $(2/\hbar)V_c$.

2.3.1 Experimental values for the average Trace-Squared Deviation

Let us consider the average Trace-Squared Deviation (TrSD) from true states defined in the main text,

$$\mathcal{D}(\rho_{\rm C}) \equiv \mathbb{E}\left[\mathrm{Tr}[(\rho_{\rm T} - \rho_{\rm C})^2]\right] = \sum_{\mathbf{U}_{\rm F},\mathbf{O}_{\rm C}} \wp(\mathbf{U}_{\rm F},\mathbf{O}_{\rm C})\mathrm{Tr}[(\rho_{\rm T} - \rho_{\rm C})^2], \tag{S54}$$

where $\mathbb{E}$ denotes an ensemble average over the true states (or equivalently over all the measurement records), the subscript $\mathrm{C} = \mathrm{F}, \mathrm{S}$ denotes either a filtered or smoothed conditioning, with $\mathbf{O}_{\rm F}$ denoting Alice's past measurement record and $\mathbf{O}_{\rm S}$ denoting the past-future record. Similar notation is used for Bob's record $\mathbf{U}$. By expanding the term in the trace, one obtains

$$\mathcal{D}(\rho_{\rm C}) = \sum_{\mathbf{U}_{\rm F},\mathbf{O}_{\rm C}} \wp(\mathbf{U}_{\rm F},\mathbf{O}_{\rm C})\left(\mathrm{Tr}[\rho_{\rm T}^2] - 2\mathrm{Tr}[\rho_{\rm T}\rho_{\rm C}] + \mathrm{Tr}[\rho_{\rm C}^2]\right) \tag{S55}$$

$$= \sum_{\mathbf{U}_{\rm F},\mathbf{O}_{\rm C}} \wp(\mathbf{U}_{\rm F},\mathbf{O}_{\rm C})\left(\mathcal{P}(\rho_{\rm T}) - 2\mathrm{Tr}[\rho_{\rm T}\rho_{\rm C}] + \mathcal{P}(\rho_{\rm C})\right), \tag{S56}$$

where the purity is defined as $\mathcal{P}(\rho) = \mathrm{Tr}[\rho^2]$. Since we are dealing with continuous-variable quantum states, it is more useful to express the quantum state in terms of its corresponding Wigner quasiprobability distribution $W(\mathbf{x})$. Using the property for a single mode system[4] that $\mathrm{Tr}[\hat{A}\hat{B}] = 2\hbar\pi\int \mathrm{d}^2\mathbf{x} W_{\rm A}(\mathbf{x})W_{\rm B}(\mathbf{x})$ and assuming Gaussian Wigner distributions, we obtain

$$\mathcal{D}(\rho_{\rm C}) = \sum_{\mathbf{U}_{\rm F},\mathbf{O}_{\rm C}} \wp(\mathbf{U}_{\rm F},\mathbf{O}_{\rm C})\left(\frac{\hbar}{2\sqrt{|V_{\rm T}|}} - 4\hbar\pi g(\langle\hat{\mathbf{x}}\rangle_{\rm T};\langle\hat{\mathbf{x}}\rangle_{\rm C}, V_{\rm T}+V_{\rm C}) + \frac{\hbar}{2\sqrt{|V_{\rm C}|}}\right), \tag{S57}$$

where $g(\mathbf{x},\mu,V)$ denotes a normalized Gaussian of a mean μ and a covariance matrix V and we have used $\int \mathrm{d}^2\mathbf{x} g(\mathbf{x};\mu,A)g(\mathbf{x};\nu,B) = g(\mu;\nu,A+B)$. Noting that the covariance matrix does not depend on either $\mathbf{U}$ or $\mathbf{O}$, we end up with

$$\mathcal{D}(\rho_{\rm C}) = \frac{\hbar}{2}(\sqrt{|V_{\rm T}|^{-1}} + \sqrt{|V_{\rm C}|^{-1}}) - 4\hbar\pi \sum_{\mathbf{U}_{\rm F},\mathbf{O}_{\rm C}} \wp(\mathbf{U}_{\rm F},\mathbf{O}_{\rm C})g(\langle\hat{\mathbf{x}}\rangle_{\rm T};\langle\hat{\mathbf{x}}\rangle_{\rm C}, V_{\rm T}+V_{\rm C}), \tag{S58}$$

which is the expression we use to compute the average TrSD from the experimental data.

2.3.2 Theoretical values for the average Trace-Squared Deviation

To derive the theoretical value for the average TrSD, let us return to (S56). Using the fact[8] that $\rho_{\mathrm{C}} = \sum_{\mathbf{U}_{\mathrm{F}}} \wp(\mathbf{U}_{\mathrm{F}}|\mathbf{O}_{\mathrm{C}})\rho_{\mathrm{T}}$ and that $\wp(\mathbf{U}_{\mathrm{F}}, \mathbf{O}_{\mathrm{C}}) = \wp(\mathbf{U}_{\mathrm{F}}|\mathbf{O}_{\mathrm{C}})\wp(\mathbf{O}_{\mathrm{C}})$, we can simplify (S56) to

$$\mathcal{D}(\rho_{\mathrm{C}}) = \sum_{\mathbf{O}_{\mathrm{C}}} \wp(\mathbf{O}_{\mathrm{C}}) \left(\mathcal{P}(\rho_{\mathrm{T}}) - 2\mathrm{Tr}[\rho_{\mathrm{C}}^2] + \mathcal{P}(\rho_{\mathrm{C}})\right) \tag{S59}$$

$$= \sum_{\mathbf{O}_{\mathrm{C}}} \wp(\mathbf{O}_{\mathrm{C}}) \left(\mathcal{P}(\rho_{\mathrm{T}}) - \mathcal{P}(\rho_{\mathrm{C}})\right) \tag{S60}$$

$$= \frac{\hbar}{2}\left(\sqrt{|V_{\mathrm{T}}|^{-1}} - \sqrt{|V_{\mathrm{C}}|^{-1}}\right), \tag{S61}$$

where, in the final line, we have used the fact that the covariance matrix is independent of the particular measurement record obtained.

2.4 Squeezing of true states

Here we show the squeezing of the true state, i.e., the uncertainty in the squeezed quadrature of the true states, as functions of Alice's and Bob's measurement angles in Fig. S3. Both the theory prediction as well as the experimental verification show that the significant true-state squeezing occurs when Bob measures a quadrature that is anti-correlated with Alice's (i.e., $\theta_{\mathrm{B}} \approx 180^\circ - \theta_{\mathrm{A}}$).

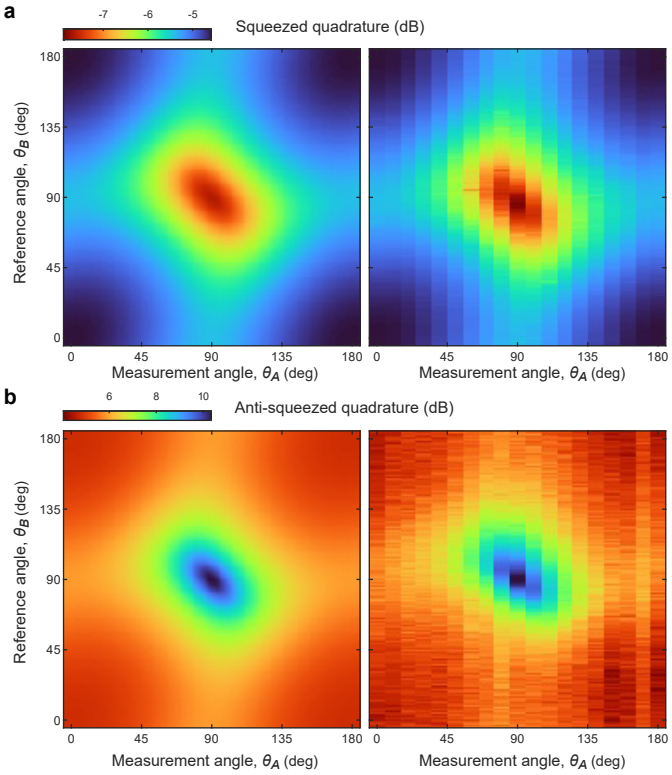


Fig. S3 The amount of squeezing and anti-squeezing, i.e., the uncertainty in the squeezed quadrature of the true state, $\mathcal{S}(\rho_{\mathrm{T}})$, in **a**, and the anti-squeezed quadrature of the true state, $\mathcal{A}(\rho_{\mathrm{T}})$, in **b**, for different values of θ_{A} and θ_{B}. Left is the theory prediction and right is the experimental verification.

2.5 Pump-amplitude dependence of the maximum purity and squeezing recoveries

Here we show the dependence of the maximum purity and squeezing recoveries on the normalized pump amplitude ξ. The purity and squeezing recoveries are defined as $\mathcal{R}_{\mathcal{P}} = \mathcal{P}(\rho_{\mathrm{S}}) - \mathcal{P}(\rho_{\mathrm{F}})$ and $\mathcal{R}_{\mathcal{S}} = \mathcal{S}(\rho_{\mathrm{F}}) - \mathcal{S}(\rho_{\mathrm{S}})$, respectively. For each value of ξ, we maximize each absolute recovery independently over Alice's and Bob's

homodyne measurement angles, θ_{A} and θ_{B}. The resulting maximum recovery is then normalized by the total recoverable difference between the true and filtered states, evaluated at the same optimal measurement angles. Specifically, the quantities plotted in Fig. S4 are

$$\widetilde{\mathcal{R}}^{\max}_{\mathcal{P}}(\xi) = \left.\frac{\mathcal{P}(\rho_{\mathrm{S}}) - \mathcal{P}(\rho_{\mathrm{F}})}{\mathcal{P}(\rho_{\mathrm{T}}) - \mathcal{P}(\rho_{\mathrm{F}})}\right|_{(\theta_{\mathrm{A}},\theta_{\mathrm{B}})=(\theta^{\mathcal{P}}_{\mathrm{A}},\theta^{\mathcal{P}}_{\mathrm{B}})}, \tag{S62}$$

$$\widetilde{\mathcal{R}}^{\max}_{\mathcal{S}}(\xi) = \left.\frac{\mathcal{S}(\rho_{\mathrm{F}}) - \mathcal{S}(\rho_{\mathrm{S}})}{\mathcal{S}(\rho_{\mathrm{F}}) - \mathcal{S}(\rho_{\mathrm{T}})}\right|_{(\theta_{\mathrm{A}},\theta_{\mathrm{B}})=(\theta^{\mathcal{S}}_{\mathrm{A}},\theta^{\mathcal{S}}_{\mathrm{B}})}, \tag{S63}$$

where $(\theta^{\mathcal{P}}_{\mathrm{A}}, \theta^{\mathcal{P}}_{\mathrm{B}})$ and $(\theta^{\mathcal{S}}_{\mathrm{A}}, \theta^{\mathcal{S}}_{\mathrm{B}})$ are the measurement angles that maximize $\mathcal{R}_{\mathcal{P}}$ and $\mathcal{R}_{\mathcal{S}}$, respectively. Thus, the optimization is performed on the absolute recovery before normalization, rather than directly maximizing the normalized recovery ratio. All system and measurement parameters other than ξ are fixed to the values used for the experimental configuration.

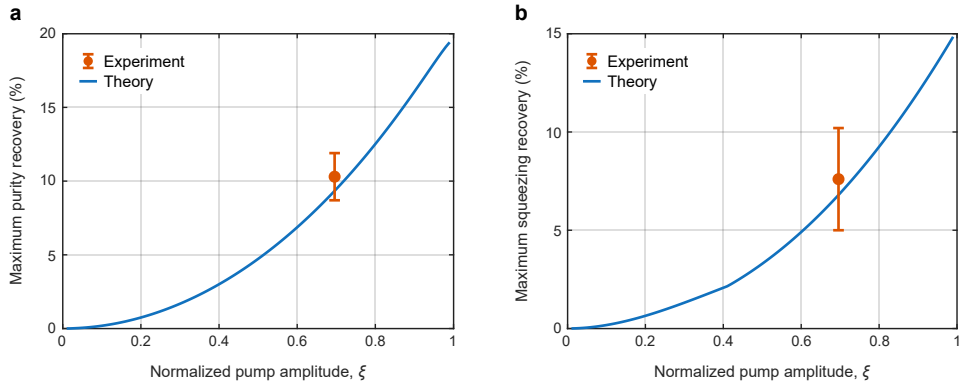


Fig. S4 Pump-amplitude dependence of the normalized maximum recoveries. a, Purity recovery. **b**, Squeezing recovery. For each ξ, the recovery is maximized over θ_{A} and θ_{B} and normalized. All other parameters are fixed to the experimental values.

References

[1] Drever, R. W. *et al.* Laser phase and frequency stabilization using an optical resonator. *Applied Physics B* **31**, 97–105 (1983).

[2] Collett, M. & Gardiner, C. Squeezing of intracavity and traveling-wave light fields produced in parametric amplification. *Physical Review A* **30**, 1386 (1984).

[3] Gardiner, C. & Zoller, P. *Quantum noise: a handbook of Markovian and non-Markovian quantum stochastic methods with applications to quantum optics* (Springer Science & Business Media, 2004).

[4] Wiseman, H. M. & Milburn, G. J. *Quantum Measurement and Control* (Cambridge University Press, 2009).

[5] Laverick, K. T., Chantasri, A. & Wiseman, H. M. Quantum state smoothing for linear Gaussian systems. *Physical Review Letters* **122**, 190402 (2019).

[6] Walls, D. F. & Milburn, G. J. *Quantum Optics* 3rd edn (Springer, 2025).

[7] Laverick, K. T., Chantasri, A. & Wiseman, H. M. Linear Gaussian quantum state smoothing: Understanding the optimal unravelings for Alice to estimate Bob's state. *Physical Review A* **103**, 012213 (2021).

[8] Guevara, I. & Wiseman, H. Quantum state smoothing. *Physical Review Letters* **115**, 180407 (2015).